

Provided for non-commercial research and education use.
Not for reproduction, distribution or commercial use.

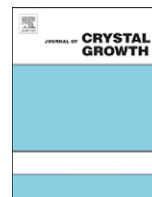


This article appeared in a journal published by Elsevier. The attached copy is furnished to the author for internal non-commercial research and education use, including for instruction at the authors institution and sharing with colleagues.

Other uses, including reproduction and distribution, or selling or licensing copies, or posting to personal, institutional or third party websites are prohibited.

In most cases authors are permitted to post their version of the article (e.g. in Word or Tex form) to their personal website or institutional repository. Authors requiring further information regarding Elsevier's archiving and manuscript policies are encouraged to visit:

<http://www.elsevier.com/copyright>



Aerosol synthesis and reactive behavior of faceted aluminum nanocrystals

Dan A. Kaplowitz^a, R.J. Jouet^b, Michael R. Zachariah^{a,*}

^a Departments of Chemistry and Biochemistry, and Mechanical Engineering, University of Maryland, College Park, MD 20740, United States

^b Indian Head Division-Naval Surface Warfare Center, Research and Technology Department, 101 Strauss Avenue, Indian Head, MD 20640, United States

ARTICLE INFO

Article history:

Received 10 May 2010

Received in revised form

2 September 2010

Accepted 7 September 2010

Communicated by B.A. Korgel

Available online 17 September 2010

Keywords:

A2. Growth from vapor

B1. Aerosol

B1. Metals

B1. Nanocrystals

ABSTRACT

We show a low temperature gas-phase synthesis route to produce faceted aluminum crystals in the aerosol phase. Use of triisobutylaluminum whose decomposition temperature is below the melting point of elemental aluminum enabled us to grow nanocrystals from its vapor. TEM shows both polyhedral crystalline and spherical particle morphologies, but with the addition of an annealing furnace one can significantly enhance the production of just the polyhedral particles. The results on surface passivation with oxygen suggest that these nanocrystals are less pyrophoric than the corresponding spherical aluminum nanoparticles, and combustion tests show an increase in energy release compared to commercial nanoaluminum.

© 2010 Elsevier B.V. All rights reserved.

1. Introduction

Metal/oxidizer combinations are being studied as energetic materials due to their high total energy content compared to CHNO based materials [1]. The high energy density of metals make them useful for propellant applications where a large rapid energy release is desired [2]. Though bulk aluminum has very high energy density for oxidation of alumina, problems arise for energetic applications because the kinetics are diffusion limited between oxidizer and aluminum. This is partially mitigated by going to smaller particles sizes in order to increase the surface to volume ratio of the aluminum particle. Decreasing particle size to the nanometer range yields a substantial increase in the surface area compared to the particles of micron size and can substantially increase reaction rate. Almost all reactive metals for example become pyrophoric for particles under 100 nm.

Nanoaluminum is by far the most important reactive metal due to its high heat of reaction to the oxide, and its low material cost. Park et al. [3] explored several methods for the production of nanoaluminum in aerosol form. Al was evaporated from solid pellets via the DC-arc discharge method that created nanoparticles upon quenching with argon gas. A second method used laser ablation to create a local microplasma on aluminum pellets that again yielded nanoparticles after an argon quench. Exploding wire has also been extensively employed for gas-phase production of nanoaluminum [4–7]. This technique uses a high density current

pulsed through an Al wire to create a microplasma, which yields ultrafine aluminum after a quench. Sindhu et al. [8] combined experimental and modeling studies to fully characterize the explosive Al wire process. Anderson and Foley. [9] investigated gas atomization reaction synthesis (GARS) for Al, a powder production technique where the molten metal is atomized in an environment of ultrahigh purity inert gas. This allows for the growth of an extremely thin oxide coating on the Al product compared to particles made from commercial air atomization (CAA) or commercial inert gas atomization (CIGA).

These methods while seeming to be very different all essentially involve very high temperature evaporation of elemental aluminum followed by a rapid quench. Not surprising, then, that these methods tend to produce similar types of polycrystalline particles with primary particle sizes less than ~50 nm, that are highly aggregated.

Low temperature routes have been successfully developed for decomposition of aluminum compounds in solution. Jouet et al. [10] catalytically decomposed in liquid phase $H_3Al \cdot NMe_3$ in organic solvents under inert gas. The bare nanoaluminum product was then surface passivated with a perfluoroalkyl carboxylic acid self-assembled monolayer to prevent oxidation. Other successful liquid phase production methods include reaction of $LiAlH_4$ with $AlCl_3$ [11], hydrogenolysis of $(AlCp^*)_4$ [12], thermal decomposition of alane N,N -dimethylethylamine [13], and several other techniques.

In this paper we explore a low temperature gas-phase route, through the use of a metal organic precursor that has a decomposition temperature below the melting point of aluminum, as a means to more carefully control the nucleation and

* Corresponding author.

E-mail address: mrz@umd.edu (M.R. Zachariah).

growth of nanoaluminum. We will demonstrate that thermal decomposition of triisobutylaluminum (TiBAI), under the appropriate time/temperature histories, can generate highly faceted nanocrystals of aluminum. These materials are then tested for their reactivity relative to conventional nanoaluminum.

2. Experimental approach

Our choice of precursor was specifically targeted to create vapor phase reaction products containing aluminum or elemental aluminum below the melting point of aluminum (660 °C) so that particle growth occurs at or near a solid like state.

TiBAI was chosen as the precursor due to its relatively low decomposition temperature. Previous work on chemical vapor deposition has shown that TiBAI can be decomposed at temperatures in the range of 250 °C to deposit thin films of aluminum with little carbon contamination [14–16]. This low decomposition temperature and its relatively high vapor pressure are both highly desirable properties for scale-up of aluminum production in large quantities. The mechanism of TiBAI decomposition also has been explored in the previous CVD work and involves deposition on the substrate, β -hydride elimination, and finally liberation of isobutylene and hydrogen, leaving elemental aluminum on the substrate. Due to the substrate's role in β -hydride elimination, it is not clear whether the mechanism and energetics for gas-phase aluminum production will be comparable. However, our efforts with triethylaluminum as the precursor yielded incomplete decomposition, suggesting that isobutylene is a better leaving group than ethylene, and thus further supporting β -hydride elimination mechanism.

3. Experimental setup

The synthesis scheme involves a continuous flow aerosol reactor. The precursor delivery system consists of a heated stainless steel bubbler filled with the liquid TiBAI precursor, through which a mass-flow metered argon flow is bubbled. Temperature control is monitored with a thermocouple placed in a thermowell built into the bubbler. Typical operating conditions of flow rate and temperature are presented in Table 1. Assuming complete vapor saturation of the argon flow based on the known vapor pressure of TiBAI the expected aluminum production rates are shown in Table 1.

Though increasing bubbler temperature by only 10 °C yields a substantial increase in theoretical production rate, temperatures were not raised above 70 °C to avoid any significant decomposition of the precursor [17].

Since both the precursor and the aluminum nanoparticle product are highly air and water sensitive, the flow train was valved so as to allow flushing with argon prior to and after each experiment. The entire flow train was heat jacketed to prevent any condensation of the precursor prior to the flow reactor. The synthesis system consists of two reactors in series, with 1 and 1/2 in. diameter quartz tubes, respectively, each heated within 15.5 in. tube furnaces. Experiments with a flow rate of 3 lpm

through the first reactor yield a residence time of 4.0 s, while a flow rate of 1.5 lpm through the second reactor after a dump gives a residence time of 2.0 s. The use of a second furnace was found to be a necessary condition to maximize the fraction of nanocrystals, relative to spherical nanoparticles.

A schematic representation of the experimental setup is shown in Fig. 1. Particles exiting the reactor were collected on Sterlitech 47 mm polypropylene membrane filters with a pore size of 200 nm in a Millipore stainless steel filter holder. Since the particles produced are oxygen free they were highly reactive. To harvest the particles on the filters for characterization we carefully bled in air so as to create a 1–3 nm oxide passivation shell on the particles. Product aerosol was also electrostatically deposited onto TEM grids for characterization. Size distribution measurements on the aerosol were obtained with a scanning mobility particle sizer (SMPS).

4. Results

Initial experiments with one reactor at 350 °C, an argon flow rate of 3 lpm, and a bubbler temperature of 60 °C produced a gray powder at the reactor outlet. Inspection of these particles via transmission electron microscopy with the JEOL JEM 2100F TEM/STEM showed two particle morphologies: spherical and polyhedral. Increasing the reactor temperature to 500 °C yielded primarily spherical particles. The final setup consisted of the first furnace at 350 °C with a flow rate of 3 lpm, and the second furnace for annealing at 500 °C with a flow rate of 1.5 lpm. This system produced mostly polyhedral particles as seen in Fig. 2, along with the results from the other two runs.

The images display particles of polyhedral structure with diagonal distances ranging from 50 to 100 nm as well as smaller spherical particles with diameters ranging from 25 to 50 nm. Spherical and polyhedral particles were counted from TEM images for the reaction conditions shown in Fig. 2(a) and (c) in order to compare the results. The single-furnace experiment at 350 °C and an Ar flow of 3 lpm yielded 46.6% polyhedral particles, whereas the two-furnace setup significantly raised the count to 92.0%.

To investigate the composition of the polyhedral particles, high resolution imagery and energy dispersive spectrometry (EDS) were employed, as shown in Fig. 3.

The high resolution images show the crystalline phase in the middle of the particle as well as an amorphous coating of ~4 nm. Line spacing measurements of 0.228 nm in the crystalline phase are consistent with the literature value of 0.233 nm for $\langle 111 \rangle$ crystalline aluminum. To confirm, diffraction patterns and EDS line scans were obtained for the product and are shown in Figs. 4 and 5.

The line scan of a polyhedral particle exhibits a clear peak of aluminum, no rise in carbon intensity, and a slight increase of oxygen intensity at the edges of the particle. The experimental diffraction pattern shows clear diffraction rings, with the first three ring diameters from the center yielding lattice spacings of 0.239, 0.201, and 0.143 nm, respectively. These match with crystalline aluminum lattice distances of 0.233, 0.203, and 0.143 nm for the $\langle 111 \rangle$, $\langle 200 \rangle$, and $\langle 220 \rangle$ planes, respectively. This information combined with the measurements from the high resolution image leads to the conclusion that the polyhedral particles are crystalline aluminum with an amorphous aluminum oxide coating. This same particle morphology was previously shown by Haber and Buhro [11] during the production of nanoAl by decomposition of aluminum containing compounds in solution. However, the previous work yielded polyhedral particles only as a small fraction of the product, whereas here

Table 1
Theoretical production rates for TiBAI decomposition.

Flow (lpm)	T (°C)	V _p (Pa)	TiBAI (mg/h)	Al (mg/h)
1.5	50	122.6	815.1	110.9
	60	281.3	1813.5	246.6
	70	439.9	2753.4	374.5

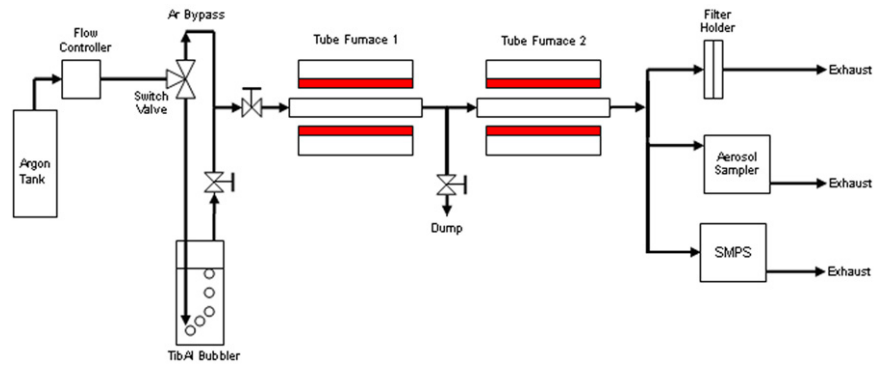


Fig. 1. Schematic representation of aerosol synthesis system of aluminum nanocrystals.

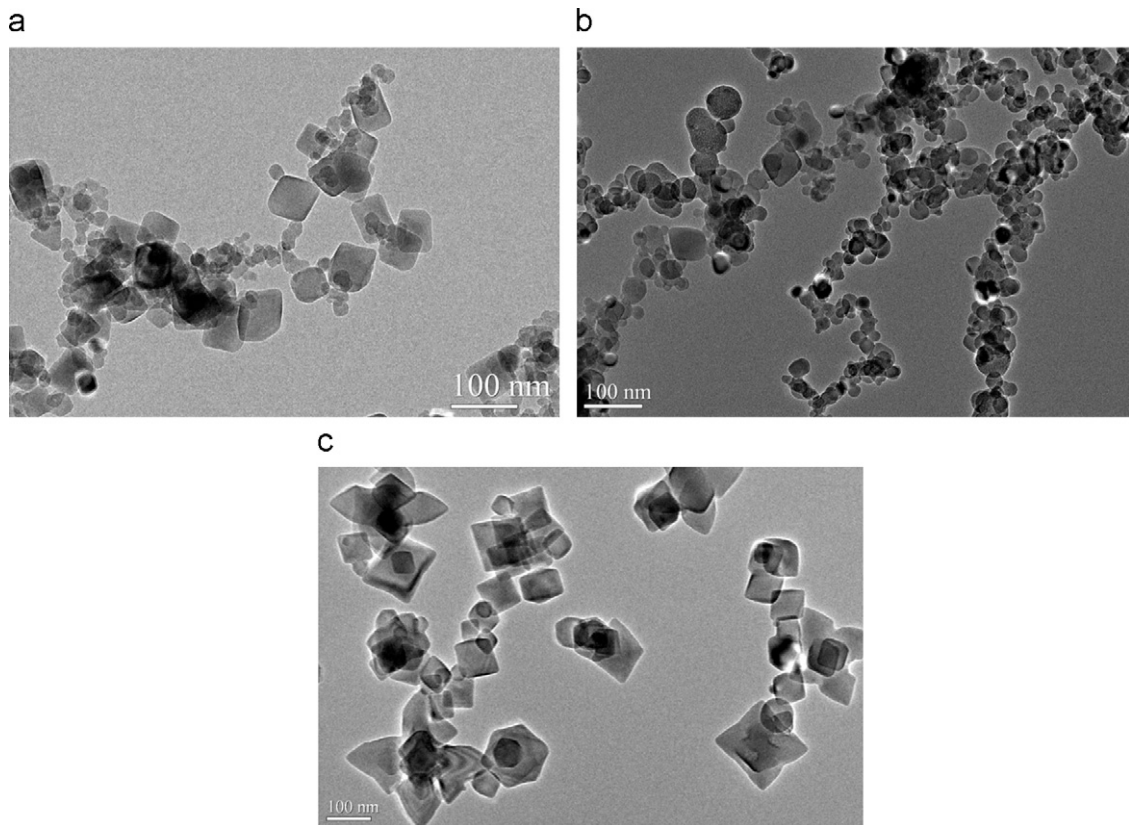


Fig. 2. TEM image of Al particles produced from three different setups: (a) one furnace 350 °C Ar flow 3 lpm; (b) one furnace 500 °C Ar flow 3 lpm; and (c) furnace 1 at 350 °C Ar flow 3 lpm and furnace 2 at 500 °C Ar flow 1.5 lpm.

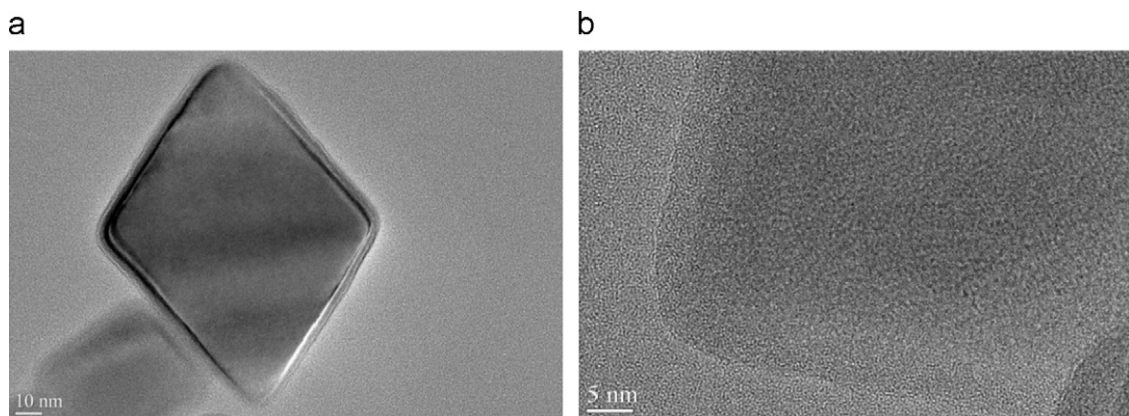


Fig. 3. High resolution TEM images of rectangular particle show a ~4 nm oxide shell formed during the air bleed.

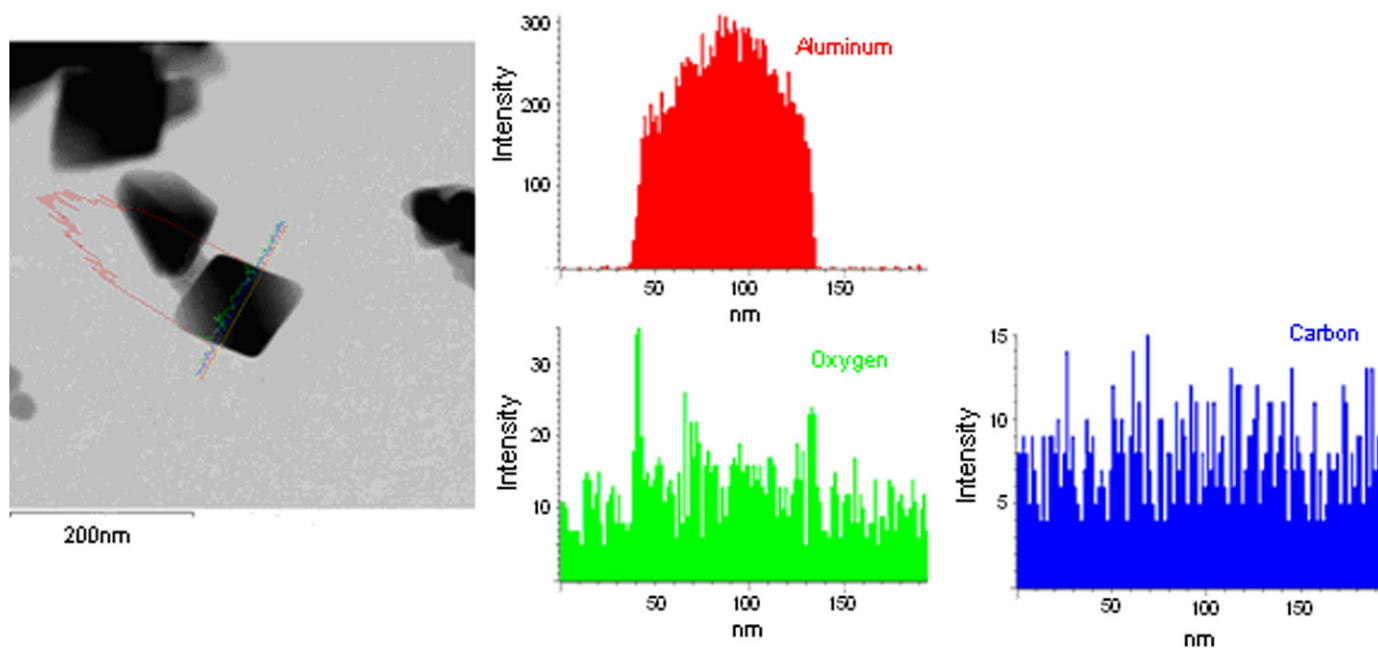


Fig. 4. EDS line scan of polyhedral particle comparing aluminum, oxygen, and carbon intensities for particles deposited on a Ni grid with SiO/SiO₂ film.

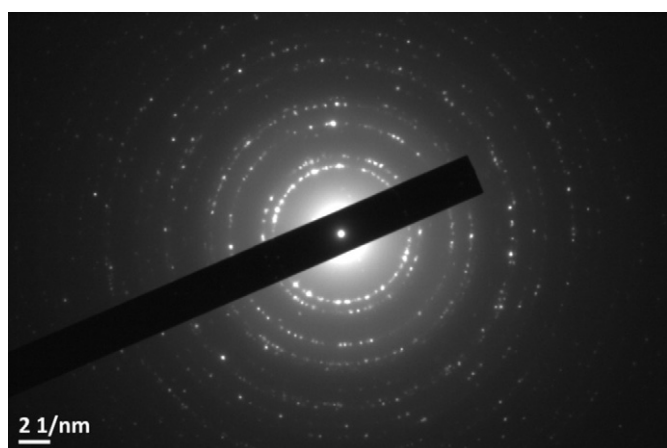


Fig. 5. X-ray diffraction image of polyhedral crystalline particle sample.

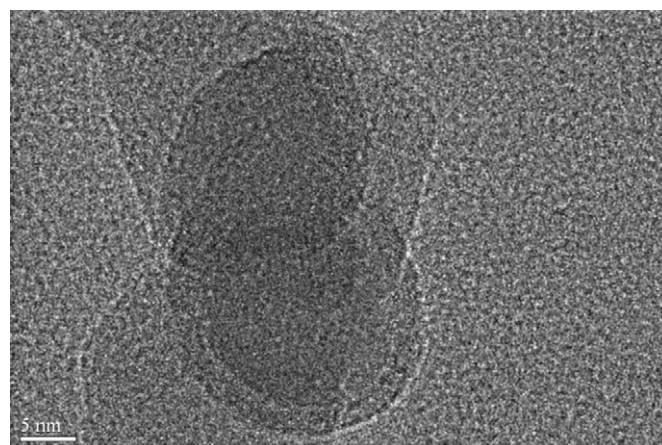


Fig. 6. High resolution TEM image of a spherical particle.

they are the major component. The key to production of mainly polyhedral crystalline particles is the addition of the second furnace to allow the spherical particles to anneal and grow in the crystal phase.

The spherical particles seen in Fig. 2(a) and (b) were originally hypothesized to be amorphous carbon contamination particles that had formed during the cracking of TiBAI. However, attempts at carbon reduction by hydrogen addition at concentrations of up to 10 mass% showed no discernable effect. High resolution images and EDS line scans of the spherical particles are shown in Figs. 6 and 7.

The high resolution image in Fig. 6 shows a mostly amorphous character. The line scan in Fig. 7 confirms that it is aluminum oxide with little carbon contamination. Since oxygen is not available to the particles until the outlet of the production system, it can be concluded that these small spherical aluminum particles are extremely reactive and that even with our oxygen bleed they have in most cases fully reacted with oxygen upon exposure. There are still parts in the core of some of these particles that remain unreacted aluminum, causing crystal lattice lines in the high resolution images. This could be an indication that these

spherical particles were pure aluminum before exposure and reaction with oxygen. When process conditions were changed to yield mostly spherical particles, the resulting samples burned completely upon exposure, even after the slow air bleed. Samples produced with mostly polyhedral crystalline particles, however did not burn upon exposure after the bleed. This suggests that these crystals have higher stability than the spherical particles.

In order to further investigate the reactivity of the polyhedral crystalline particles, samples were combined with stoichiometric CuO and burned in a pressure cell; a closed stainless steel chamber with ports connected for measurement of optical and pressure response during combustion. The resulting optical response is compared to a response from commercial aluminum/CuO in Fig. 8. The commercial aluminum, obtained from Argonide Corporation, has average diameter ~ 50 nm and contained $\sim 70\%$ unreacted aluminum as determined by TGA.

The broader peak for the synthesized aluminum suggests that either the polyhedral crystalline particles ignite at a higher temperature after the spherical particles in the sample have started burning or the polyhedral particles actually have longer

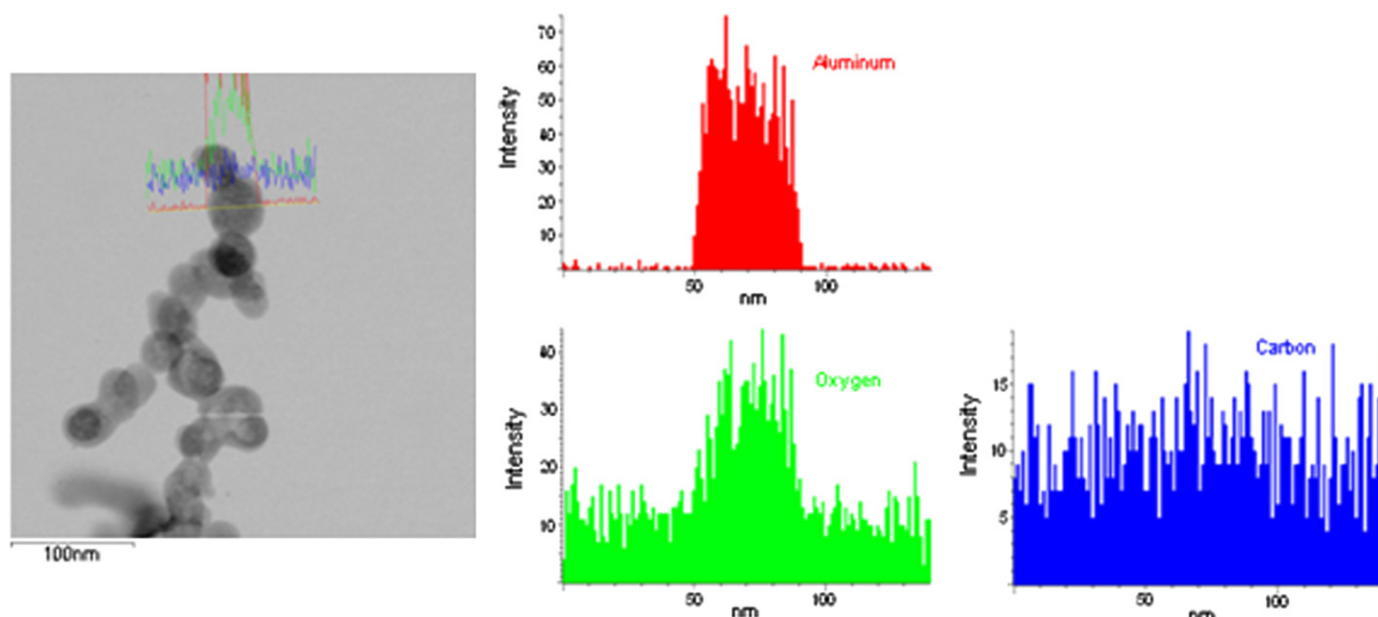


Fig. 7. EDS line scan of spherical particle comparing aluminum (red), oxygen (green), and carbon (blue) intensities for particles deposited on a Ni grid with SiO/SiO₂ film. (For interpretation of the references to colour in this figure legend, the reader is referred to the web version of this article.)

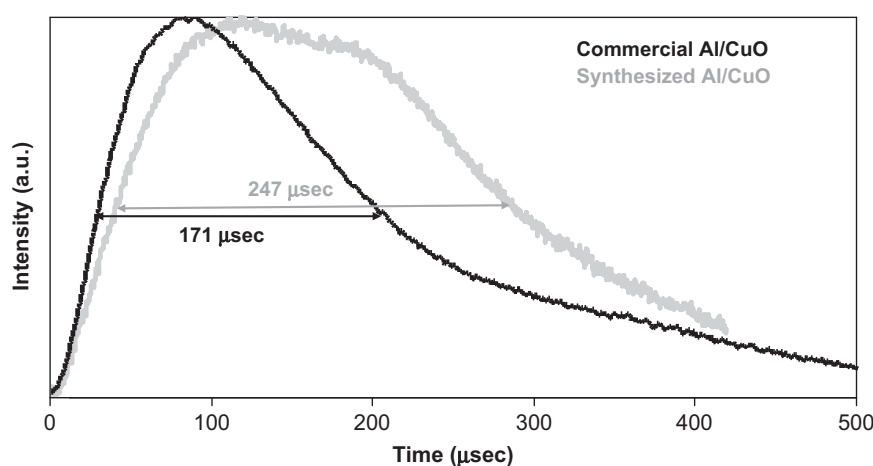


Fig. 8. Optical response from combustion of commercial (black) and synthesized (gray) aluminum with stoichiometric CuO in pressure cell test.

burn times than standard nanoaluminum. This result is consistent with the previous observation that the polyhedral crystal particles were not as pyrophoric as spherical particles produced with our system. The enhanced stability of these particles can be attributed to the higher surface binding energy for molecules on a flat surface compared to that of a curved surface due to the Kelvin effect [18].

Pressure response from these experiments showed a maximum pressure rise of 166 psi for the synthesized Al compared to a value of 116 psi for commercial product, both with similar rise times. The polyhedral particles thus yield a significant enhancement in reactivity. This information combined with the optical and experimental observations lead to the conclusions that we have produced polyhedral nanoaluminum particles with both enhanced stability and increased energy release.

Thermal gravimetric analysis (TGA) under air was employed to further scrutinize polyhedral particle samples, specifically to determine the remaining active aluminum content after particles

had formed an oxide shell. Resulting mass measurement is shown in Fig. 9 as temperature is raised to 1200 °C at 10 °C/min then held for 30 min.

The results show an active Al content of ~64%, a value slightly lower but comparable to the 70% content measured for commercial nanoAl in TGA. This latter point probably has more to do with optimization, bringing the particle up to ambient conditions by controlled air bleeding, something we did not investigate in the work. Despite the apparent increase in oxygen content we still observe enhanced energy release upon reaction with CuO.

In-line size distributions of the aerosol aluminum product measured using a scanning mobility particle sizer yields a concentration of $\sim 3 \times 10^7$ particles/cm³, with a standard deviation of 1.6, and a geometric mean of 170 nm. However, this is a measure of aggregate size distributions and will change with particle concentration and residence time. To measure crystallite size we used TEM to create a histogram of sizes. This approach yielded a distribution with average primary particle size of ~ 87 nm and a

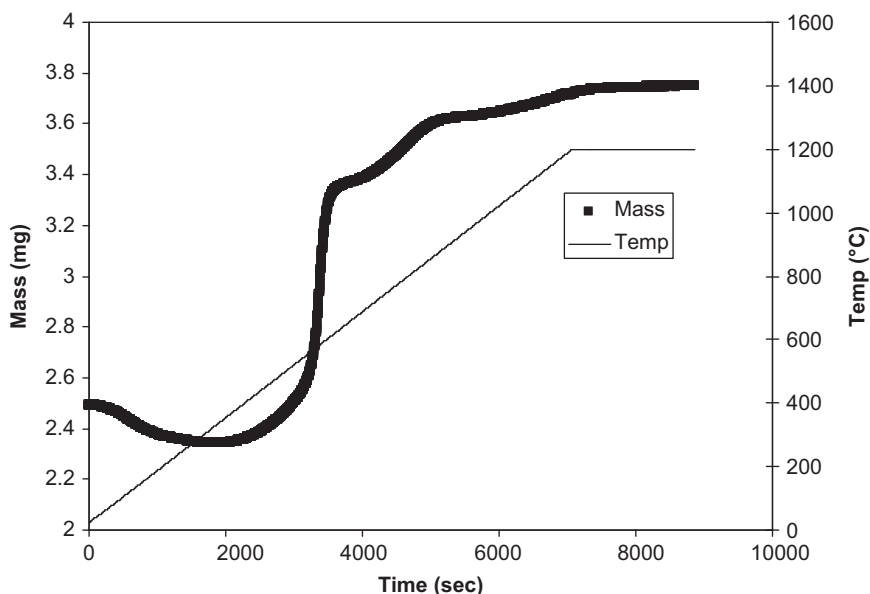


Fig. 9. TGA oxidation in air for synthesized Al sample.

standard deviation of 33 nm. Due to the polyhedral shape of the particles, diagonal distances were used as the descriptive size measurement for each particle. Since the TEM grids are open to air after collection, this distribution is for aluminum particles that have formed a thin aluminum oxide coating.

5. Conclusions

A low temperature gas-phase pyrolysis of TiBAI was used to produce phase pure bare aluminum aerosol nanocrystals. TEM shows both polyhedral crystalline and spherical particle morphologies, but addition of an annealing furnace allows for production of primarily polyhedral crystals. These particles form a ~ 4 nm oxide shell after exposure to air, and combustion studies lead to the conclusions that these polyhedral nanoaluminum particles have both enhanced stability and increased energy release. Though the bare nanoaluminum in these experiments was passivated with oxygen, this system could easily be coupled with other systems to coat the bare aluminum with other materials for specific energetic applications.

Acknowledgments

We gratefully acknowledge the support of the Defense Threat Reduction Agency, the University of Maryland Center for Energetic Concepts Development (CECD), and the Maryland NanoCenter and its NispLab. The NispLab is supported in part by the NSF as MRSEC shared experimental facility. We would also like to thank Christopher Bunker at the Air Force Research

Laboratory for detailed discussions supporting this work and assistance with characterization of the materials.

References

- [1] S.H. Fischer, M.C. Grubelich, 32nd AIAA/ASME/SAE/ASEE Joint Propulsion Conference, July 1–3, Lake Buena Vista, FL, 1996.
- [2] A. Rai, K. Park, L. Zhou, M.R. Zachariah, *Combustion Theory and Modelling* 10 (2006) 843–859.
- [3] K. Park, D. Lee, A. Rai, D. Mukherjee, M.R. Zachariah, *Journal of Physical Chemistry B* 109 (2005) 7290–7299.
- [4] T.K. Sindhu, R. Sarathi, S.R. Chakravarthy, *Bulletin of Materials Science* 30 (2007) 187–195.
- [5] Y.S. Kwon, Y.H. Jung, N.A. Yavorovsky, A.P. Illyin, J.S. Kim, *Scripta Materialia* 44 (2001) 2247–2251.
- [6] V. Ivanov, Y.A. Kotov, O.H. Samatov, R. Bohme, H.U. Karow, G. Schumacher, *Nanostructured Materials* 6 (1995) 287–290.
- [7] R. Sarathi, T.K. Sindhu, S.R. Chakravarthy, *Materials Letters* 61 (2007) 1823–1826.
- [8] T.K. Sindhu, R. Sarathi, S.R. Chakravarthy, *Nanotechnology* 19 (2008).
- [9] I.E. Anderson, J.C. Foley, *Surface and Interface Analysis* 31 (2001) 599–608.
- [10] R.J. Jouet, A.D. Warren, D.M. Rosenberg, V.J. Bellitto, K. Park, M.R. Zachariah, *Chemistry of Materials* 17 (2005) 2987–2996.
- [11] J.A. Haber, W.E. Buhro, *Journal of the American Chemical Society* 120 (1998) 10847–10855.
- [12] M. Cokoja, H. Parala, M. Schroter, A. Birkner, M.W.E. van der berg, W. Grunert, R.A. Fischer, *Chemistry of Materials* 18 (2006) 1634–1642.
- [13] K.A.S. Fernando, M.J. Smith, B.A. Harruff, W.K. Lewis, E.A. Gulians, C.E. Bunker, *Journal of Physical Chemistry Letters* 113 (2009) 500–503.
- [14] B.E. Bent, R.G. Nuzzo, L.H. Dubois, *Journal of the American Chemical Society* 111 (1989) 1634–1644.
- [15] A.W.E. Chan, R. Hoffmann, *Journal of Vacuum Science and Technology A: Vacuum Surfaces and Films* 9 (1991) 1569–1580.
- [16] D.A. Mantell, *Journal of Vacuum Science and Technology A: Vacuum Surfaces and Films* 7 (1989) 630–633.
- [17] Triisobutylaluminum: CAS 100-99-2, SC2011, Albemarle Corporation, Baton Rouge, Louisiana., 1999.
- [18] S.K. Friedlander, *Smoke, Dust, and Haze*, Oxford University Press Inc., New York, 2000, pp. 256–257.